TISSUE ENGINEERING: Part A
Volume 22, Numbers 5 and 6, 2016

DOI: 10.1089/ten.tea.2015.0355

termis
Tissue Engineering
& Regenerative Medicine
International Society

ORIGINAL ARTICLE

Effects of Recombinant Human Bone Morphogenetic Protein-2 Dose and Ceramic Composition on New Bone Formation and Space Maintenance in a Canine Mandibular Ridge Saddle Defect Model

Anne D. Talley, BS,[1] Kerem N. Kalpakci, PhD,[2] Daniel A. Shimko, PhD,[2] Katarzyna J. Zienkiewicz, MS,[1] David L. Cochran, DDS,[3] and Scott A. Guelcher, PhD[1,4,5]

Treatment of mandibular osseous defects is a significant clinical challenge. Maintenance of the height and width of the mandibular ridge is essential for placement of dental implants and restoration of normal dentition. While guided bone regeneration using protective membranes is an effective strategy for maintaining the anatomic contour of the ridge and promoting new bone formation, complications have been reported, including wound failure, seroma, and graft exposure leading to infection. In this study, we investigated injectable low-viscosity (LV) polyurethane/ceramic composites augmented with 100 μg/mL (low) or 400 μg/mL (high) recombinant human bone morphogenetic protein-2 (rhBMP-2) as space-maintaining bone grafts in a canine mandibular ridge saddle defect model. LV grafts were injected as a reactive paste that set in 5–10 min to form a solid porous composite with bulk modulus exceeding 1 MPa. We hypothesized that compression-resistant LV grafts would enhance new bone formation and maintain the anatomic contour of the mandibular ridge without the use of protective membranes. At the rhBMP-2 dose recommended for the absorbable collagen sponge carrier in dogs (400 μg/mL), LV grafts maintained the width and height of the host mandibular ridge and supported new bone formation, while at suboptimal (100 μg/mL) doses, the anatomic contour of the ridge was not maintained. These findings indicate that compression-resistant bone grafts with bulk moduli exceeding 1 MPa and rhBMP-2 doses comparable to that recommended for the collagen sponge carrier support new bone formation and maintain ridge height and width in mandibular ridge defects without protective membranes.

Introduction

Treatment of alveolar ridge atrophy and large ridge defects poses significant clinical challenges, which are compounded by the need to restore form and function through placement of dental implants. Implant surgery requires height and width of the alveolar ridge to support dental implants and restore normal dentition. A variety of bone grafts can be used to promote lateral ridge augmentation, including allogenic or autogenic bone, recombinant human growth factors, osteoconductive scaffolds, and guided bone regeneration (GBR) using degradable or nondegradable membranes.[1] However, these approaches are limited by unpredictable host bone or graft resorption, exposure of the bone graft or membrane leading to infection, and the necessity of additional surgical sites.[2] Thus, there is considerable interest in tissue engineering approaches to repair alveolar defects with the long-term goal of producing functional grafts that support simultaneous dental implant placement.

Synthetic substitutes for bone grafting include ceramics and bioactive glasses (BGs). Ceramics, such as tricalcium phosphate and hydroxyapatite (HA), have been used extensively in bone grafting for a variety of applications.[3] BGs stimulate bone regeneration due to ion dissolution and surface bonding with bone, and the original 45S5 Bioglass® has been used in more than a million patients for bone defect repair in craniomaxillofacial (CMF) and orthopedic

[1]Department of Chemical and Biomolecular Engineering, Vanderbilt University, Nashville, Tennessee.
[2]Medtronic Spinal, Memphis, Tennessee.
[3]Department of Periodontics, University of Texas Health Science Center at San Antonio, San Antonio, Texas.
[4]Department of Biomedical Engineering, Vanderbilt University, Nashville, Tennessee.
[5]Center for Bone Biology, Vanderbilt University Medical Center, Nashville, Tennessee.

applications.[4] Both ceramics and BGs are often combined with polymers to enhance their mechanical and handling properties.[5] Injectable and biodegradable lysine-derived polyurethane (PUR) scaffolds have been extensively investigated in bone regeneration applications.[6,7] When tested in femoral plug defects in rabbits, PUR/ceramic composites supported local sustained delivery of recombinant human bone morphogenetic protein-2 (rhBMP-2) leading to cellular infiltration and new bone formation.[8] The mechanical properties of PUR/ceramic composites can be tuned by varying the cross-link density of the polymer phase, making them suitable even for weight-bearing applications.[9,10]

Local delivery of synthetic growth factors has been reported to enhance healing of CMF bone defects.[11] Delivery of rhBMP-2, an osteoinductive factor that stimulates osteoblast differentiation and new bone formation, from an absorbable collagen sponge (ACS) is FDA approved for localized alveolar ridge augmentation and sinus lift procedures. Previous studies have demonstrated the efficacy of rhBMP-2 in preclinical calvarial defect models in rats[12–14] and rabbits,[7,15] preclinical lateral ridge augmentation models in dogs and nonhuman primates,[16,17] and alveolar ridge augmentation in humans.[18]

Bone grafting is often combined with GBR to maintain the anatomic contour and height of the alveolar ridge. GBR requires placement of a resorbable or nonresorbable barrier membrane around the graft to prevent soft tissue prolapse and stabilize the graft.[19–21] However, the GBR approach is limited by complications, including wound failure, seroma, and infection, as well as the potential need for a secondary surgery to remove the membrane.[16,22,23] Due to inconsistent outcomes and limitations associated with GBR, it is desirable to find a bone graft that does not require the use of membranes to maintain the defect volume during bone remodeling.

In this study, we investigated injectable low-viscosity (LV) PUR/ceramic composites augmented with 100 μg/mL (low) or 400 μg/mL (high) rhBMP-2 as space-maintaining bone grafts in a canine ridge saddle defect model. LV grafts were injected as a reactive paste that set in 5–10 min to form a solid porous composite with bulk modulus exceeding 1 MPa. We hypothesized that LV grafts would enhance new bone formation and maintain space without the use of protective membranes and that a more slowly degrading ceramic matrix would more effectively maintain the mandibular ridge height and width.

Materials and Methods

Materials

Lysine triisocyanate-poly(ethylene glycol) prepolymer (LTI-PEG, 21.7% NCO) was purchased from Ricerca Biosciences LLC (Painesville, OH). Glycerol, stannous octoate, ε-caprolactone, and APTES were purchased from Sigma-Aldrich (St. Louis, MO). Glycolide and DL-lactide were supplied by Polysciences (Warrington, PA). Triethylene diamine (TEDA) and dipropylene glycol (DPG) were purchased from Sigma-Aldrich and mixed to obtain a 10% (w/w) solution of TEDA in dry DPG. MASTERGRAFT® Mini Granules (ceramic [CM]) were received from Medtronic Spinal (Memphis, TN). 45S5 BG particles (150–212 μm) were purchased from Mo-Sci Corporation (Rolla, MO). The rhBMP-2 was received from Medtronic Spinal.

Synthesis of polyester triol

The polyester triol was synthesized as described previously.[24,25] Briefly, glycerol was mixed with ε-caprolactone, glycolide, and DL-lactide monomers under argon at 140°C for 40 h. The resulting polyester triol was cooled, washed with hexane, and vacuum-dried at 80°C. The backbone of the polyester consisted of 70% ε-caprolactone, 20% glycolide, and 10% DL-lactide, and the molecular weight was 450 g/mol.

Surface modification of BG

The surface of the BG particles was modified as described previously to ensure adequate interfacial bonding and mechanical properties.[10,26–28] Briefly, melt-derived 45S5 BG particles were cleaned via sonication in acetone in deionized (DI) water (95 vol%) and subsequently sonicated three times in DI water to rinse the particles. Next, particles were silanized via a solution of APTES for 5 h at room temperature, rinsed with ethanol, and annealed at 100°C for 1 h. For surface-initiated ring-opening polymerization, a mixture comprising a 1:1000 M ratio of Sn(Oct)2:dried ε-caprolactone and a 0.83:1 weight ratio of Sil-BG:ε-caprolactone was reacted while stirring at 110°C. The polymerization time of 24 h corresponded to a final poly(ε-caprolactone) (PCL) molecular weight of 19,225 g/mol. Finally, nongrafted PCL was extracted with chloroform, and particles were dried at 40°C for 24 h.

Fabrication of LV bone grafts

CM granules were ground and sieved to 100–500 μm. The components of the LV grafts were mixed in a two-step method. In the first step, the polyester triol, particles (either 45 wt% CM or 45 wt% BG), and TEDA (1.1 pphp) were added to a 10-mL cup and mixed by hand for 30 s. The LTI-PEG and lyophilized rhBMP-2 were added to the cup and mixed by hand for 60 s. The index (ratio of isocyanate:hydroxide equivalents ×100) was 115. For material characterization, the reactive mixture was mixed with 3 pphp of DI water (to simulate *in vivo* curing in the presence of moisture), loaded into a straight bore syringe, and injected into a 6-mm vial. These samples were allowed to cure for 24 h before cutting.

Characterization of physical and mechanical properties

Composite bone grafts were cut into sections, mounted onto a scanning electron microscopy (SEM) Pin Stub Mount, and sputter coated for 40 s using a Cressington Q108 sputter coater, which deposited gold at a 30 mA current. A Hitachi S-4200 SEM was used to acquire images at a voltage of 1 kV. Images ($n = 3$ per formulation) were analyzed for pore size using ImageJ 1.47p image analysis software. Cylindrical samples with 6 mm diameter and lengths of ~12 mm were prepared with porosities of ~50% (measured gravimetrically).

Samples were submerged in phosphate-buffered saline for 24 h before mechanical testing. Compression testing was performed using an MTS 898 Bionix System (Eden Prairie, MN) with a 1 kN load cell. Samples were preloaded to 3 N and compressed at a constant rate of 25 mm/min. The original cross-sectional area of the cylinders was used to calculate compressive stress. The compressive strength was reported at sample failure, and the bulk (compressive) modulus was calculated as the slope of the initial linear portion of the

Table 1. Treatment Groups Evaluated in the Canine Mandibular Ridge Saddle Defects

Treatment group	*Particle*	*Particle diameter (μm)*	*rhBMP-2 μg·cm^{-3} defect volume*	n
LV/BG-L	Bioactive glass	150–212	100	6
LV/BG-H	Bioactive glass	150–212	400	6
LV/CM-L	MASTERGRAFT	100–500	100	6
LV/CM-H	MASTERGRAFT	100–500	400	6

rhBMP-2, recombinant human bone morphogenetic protein-2.

stress–strain curve. Porosity, pore size, and compression data are presented as mean ± standard deviation of triplicate samples.

Evaluation of LV bone grafts in a canine mandibular ridge saddle defect model

Six skeletally mature hounds were used in this study. All surgical and care procedures were carried out under aseptic conditions according to the approved IACUC protocol. Treatment groups are listed in Table 1. The individual components of the LV grafts were gamma-irradiated using a dose of 25 kGY. In the first surgery, the dogs underwent bilateral extraction of the four mandibular premolars and first molar (Fig. 1A). After at least a 2-month healing period, a second surgery was performed to create two saddle defects bilaterally in each mandible (four defects per dog) measuring ~7–10 mm mesiodistally, 6–8 mm apicocoronally, and 8–10 mm buccolingually (Fig. 1B). A soft tissue pocket was created by stitching the gingiva on the mesiodistal boundaries of the defect (Fig. 1C). The LV bone grafts were mixed with rhBMP-2 and injected into the soft tissue pocket at the defect site (Fig. 1D) and allowed to cure for 10 min before soft tissue closure (Fig. 1E). Defects were filled with LV/CM or LV/BG at a low (100 μg/mL) or a high (400 μg/mL) dose of rhBMP-2 ($n = 6$ per group). The dogs were euthanized after 16 weeks. The mandibles were extracted (Fig. 1F) and fixed in 10% formalin for 2 weeks before processing for histology.

Analysis of bone morphometry by micro-computed tomography

A μCT50 (SCANCO Medical, Bassersdorf, Switzerland) was used to acquire scans of the extracted mandibles in

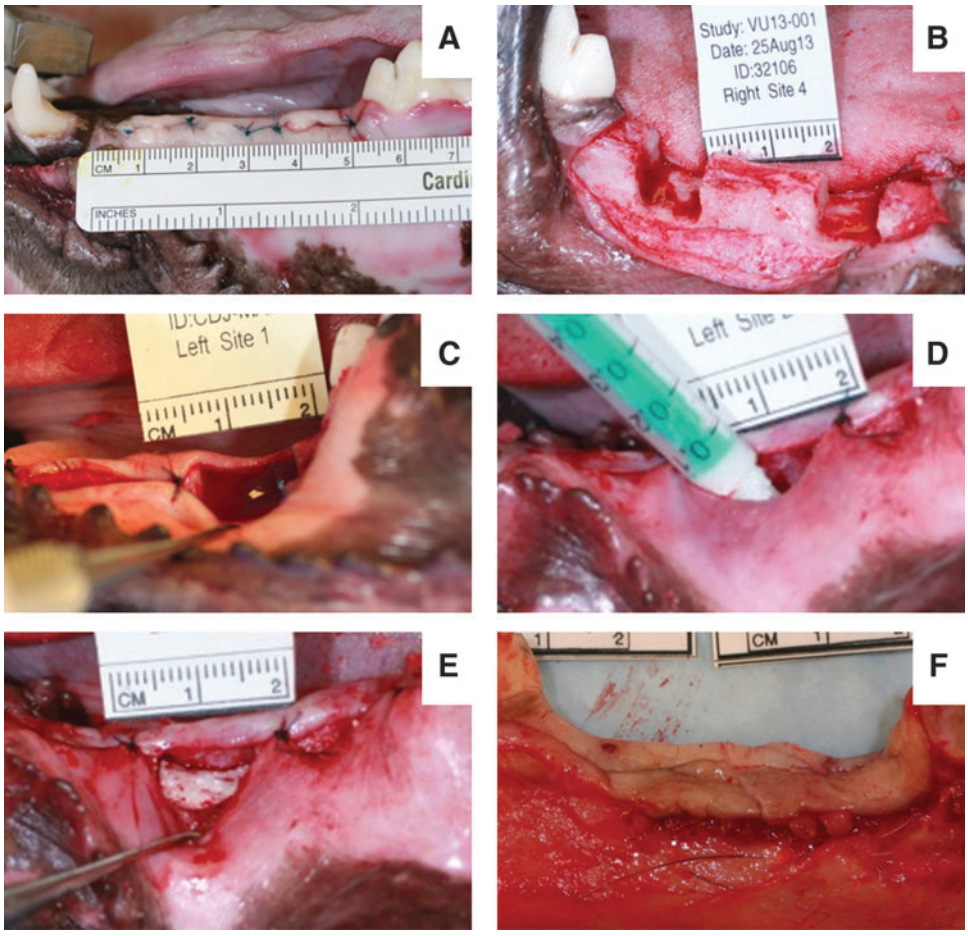

FIG. 1. Surgical photographs. **(A)** Tooth extraction surgery. **(B)** Second surgery to create the saddle defect in the mandibular ridge. **(C)** Creation of a soft tissue pocket around defect site. **(D)** Injection of low-viscosity (LV) grafts in the saddle defects. **(E)** LV graft after the polyurethane (PUR) reaction. **(F)** Mandibular ridge following canine sacrifice and bone extraction. Color images available online at www.liebertpub.com/tea

Table 2. Physical and Mechanical Properties of LV Composites

Treatment group	*Porosity (%)*	*Pore diameter (μm)*	*Bulk modulus (MPa)*	*Yield strength (MPa)*	*Yield strain (%)*
LV/BG	52.4 ± 0.3	88.6 ± 2.2[a]	1.2 ± 0.1[a]	0.37 ± 0.03	27.4 ± 5.2[a]
LV/CM	48.0 ± 3.0	100.1 ± 1.2	3.1 ± 0.4	0.38 ± 0.05	16.5 ± 4.2

[a]Significantly different at $p < 0.05$.

formalin at 70 kVp energy, 200 μA source current, 1000 projections per rotation, 800 ms integration time, and an isotropic voxel size of 24.2 μm. Axial images were reconstituted using manufacturer-provided software. Attenuation values were converted to tissue mineral density through calibration with HA phantoms with densities of 0–780 mg HA cm^{-3} (calibrations checked weekly). Using the coronal boundary of the defect for alignment, the reconstructed image stack was reoriented so that the apicocoronal direction was parallel to the z-axis. Ridge width in the defect (buccolingual direction) was measured at 2-mm intervals up to a total distance of 6 mm from the coronal base of the defect. Ridge width within the defect area was normalized to host bone ridge width on either side of the defect. Maximum ridge height (apicocoronal direction) was measured at the mesiodistal center of the defect for each sample.

Morphometric parameters were measured in a region of interest measuring 10 mm (mesiodistally) × 3 mm (buccolingually) × 3 mm (apicocoronally). Ossified tissue was segmented from soft tissue using the lower and upper thresholds of 240 mg HA cm^{-3} and 1000 mg HA cm^{-3}, respectively, with a Gaussian noise filter settings of sigma 0.7 and support 2. Bone volume/total volume (BV/TV), trabecular number (Tb.N.), trabecular thickness (Tb.Th.), and trabecular separation (Tb.Sp.) within the regions of interest were computed using SCANCO Medical μCT systems software as described previously.[29]

Histology

After fixation in formalin, the explanted mandibles were dehydrated in a graded series of ethanol and embedded in poly(methylmethacrylate) (PMMA). Using an Exakt band saw, sections were cut from each block in the center of the defect (buccolingually) using the micro-computed tomography (μCT) images as reference. The sections were then ground and polished to <100 μm using an Exakt grinding system and stained with Sanderson's rapid bone stain. New bone stained red, residual CM stained black, and infiltrating cells stained blue. Residual BG particles appeared white and did not absorb the stain. Histological sections were used to measure the maximum ridge height within the defect area similar to a method previously reported[30] used for the μCT 2D sections. Measurements of the maximum ridge height (highest point within the defect area) were taken using Metamorph software (version 7.0.1, Molecular Devices, Waltham, MA). Values of maximum ridge height by both methods were plotted together for each group.

Statistical analysis

Differences in porosity, modulus, and yield strength between groups were tested for statistical significance by unpaired Student's *t*-tests. Maximum ridge height, by μCT, was analyzed by one-way ANOVA. Morphometric parameters, including BV/TV, Tb.N., Tb.Th., and Tb.Sp., were tested by one-way ANOVA. A two-way ANOVA was run to test significance of normalized ridge width data comparing among means of each group at the different vertical positions. To compare maximum ridge heights measured from μCT and histological sections, a Bland–Altman plot was constructed, in which the average value for each group is plotted against the difference between methods. Statistical significance was considered for $p < 0.05$.

Results

Composite characterization

Physical and mechanical properties of LV grafts are summarized in Table 2. Both LV/CM and LV/BG grafts exhibited initial porosities of 48–52%, which are comparable to values reported previously for allograft bone[31,32] and ceramic composites.[8] Representative SEM images (Fig. 2) show the morphology of the pores in the grafts. The ceramic particles are

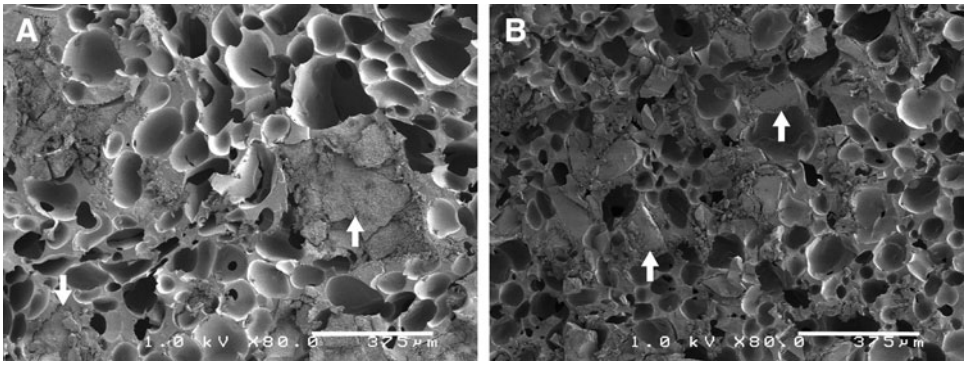

FIG. 2. Scanning electron microscopy images of **(A)** LV/CM and **(B)** LV/bioactive glass (BG) composite bone grafts. *White arrows* point to matrix particles embedded within the PUR scaffold.

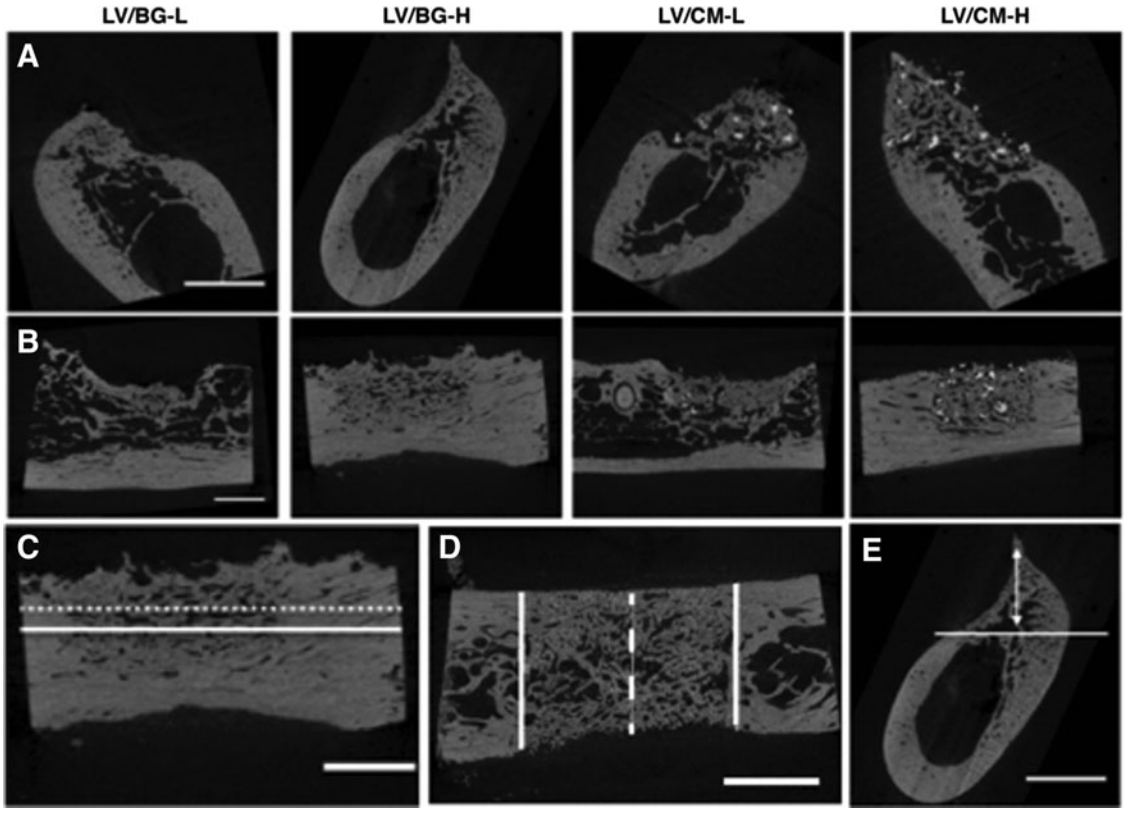

FIG. 3. Micro-computed tomography (μCT) analysis. **(A)** Representative 2D images of axial (coronal plane) cross sections. **(B)** Representative 2D images of longitudinal (sagittal plane) cross sections. **(C)** Schematic illustrating measurement of ridge width from a 2D longitudinal cross section at 2 mm (*solid line*) and 4 mm (*dotted line*) above the base of the defect. **(D)** Schematic illustrating measurement of ridge width from a 2D transverse plane cross section. Normalized ridge width was calculated as the width measured at the mesiodistal center of the defect (*dashed white* line) divided by the average width of the host bone bone (*solid white* lines). Measurements were taken at heights 2, 4, and 6 mm above the base of the defect (shown in **C**). **(E)** Representative image depicting measurement of the maximum ridge height in 2D longitudinal sections at the mesiodistal center of the defect. The *solid line* shows the base of the defect, and the *double arrow* represents the maximum ridge height. The scale bar denotes 5 mm.

embedded in the PUR network for both LV/BG and LV/CM composites. The average pore diameter was significantly higher for LV/CM composites (100.1 ± 1.2 μm) compared to LV/BG composites (88.6 ± 2.2 μm). The modulus of LV/CM composites (3.1 ± 0.4 MPa) was significantly higher than that of LV/BG composites (1.2 ± 0.1 MPa, Table 2). Additionally, the yield strain at failure was significantly higher for LV/BG composites (27.4% ± 5.2%) compared to LV/CM composites (16.5% ± 4.2%). In contrast, there were no significant differences in compressive yield strength of LV/CM (0.38 ± 0.05 MPa) and LV/BG (0.37 ± 0.03 MPa) composites.

μCT analysis

Representative 2D μCT images of axial and longitudinal cross sections of all treatment groups are presented in Figure 3. New bone is visible in the defect site for all treatment groups. Defects treated with LV/BG-L and LV/CM-L groups demonstrated less new bone and lower ridge heights than the equivalent high-dose groups. In the LV/CM samples, residual CM particles are dispersed throughout the new bone (bright white particles), whereas residual BG cannot be distinguished from new bone in the LV/BG samples. Ridge width at the mesiodistal center of the defect was measured at 2, 4, and 6 mm above the baseline of the defect (Fig. 3C) from 2D sections in the transverse plane (Fig. 3D). The normalized ridge width was calculated by dividing the width measured at the center of the defect (dashed white line in Fig. 3D) by the average width of the host bone in the ridge (solid white lines in Fig. 3D) and plotted versus height above the baseline (Fig. 4A). For defects treated with the low dose of rhBMP-2, normalized ridge width decreased with increasing ridge height. In contrast, defects treated with the high dose of rhBMP-2 maintained ridge width comparable to that of the host bone with increasing ridge height up to 6 mm above the defect baseline. At 4 mm above the base of the defect, the LV/CM-H group showed significantly greater ridge width compared to LV/BG-L. At 6 mm above the base of the defect, both high-dose treatment groups displayed significantly greater normalized ridge widths compared to the low-dose groups.

Maximum ridge heights were also measured at the mesiodistal center of the defect from axial (coronal plane) sections as illustrated in Figure 3E. The high-dose treatment groups showed significantly higher maximum ridge heights compared to the low-dose groups (Fig. 4B). There were no significant differences between LV/CM-L and LV/BG-L groups or between LV/CM-H and LV/BG-H groups. Morphometric parameters were also analyzed to assess the quality

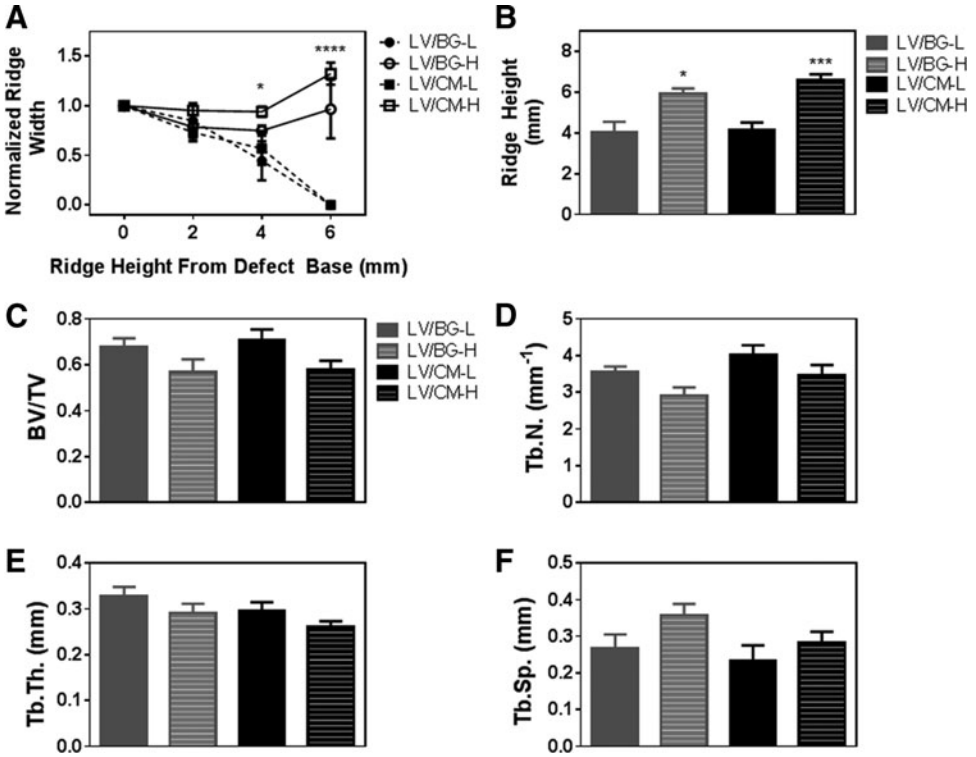

FIG. 4. Quantitative analysis of space maintenance and new bone formation by μCT. **(A)** Normalized ridge width measured at the mesiodistal center of the defect as a function of height above the baseline of the defect. Ridge width measured for the LV/CM-H group was significantly greater than that measured for the LV/BG-L at 4 mm above the base of the defect ($p < 0.05$). Both high-dose treatment groups showed significantly higher ridge heights compared to the low-dose groups at 6 mm above the base of the defect ($p < 0.0001$). **(B)** Maximum ridge height measured at the mesiodistal center of the defect. Significant differences between low- and high-dose groups are denoted by $*p < 0.05$ and $***p < 0.001$. No significant differences between LV/BG-L and LV/CM-L or between LV/CM-L and LV/CM-H were observed. **(C–F)** Morphometric parameters measured from μCT images: **(C)** bone volume/total volume (BV/TV), **(D)** trabecular number (Tb.N.), **(E)** trabecular thickness (Tb.Th.), and **(F)** trabecular separation (Tb.Sp.) No significant differences in morphometric parameters were observed between groups.

of the new bone within the defect site (Fig. 4C–F). There were no significant differences in BV/TV, Tb.N., Tb.Th., or Tb.Sp. between groups.

Histology

Figure 5 shows representative low- and high-magnification images of histological sections for all treatment groups. With Sanderson's rapid bone stain, new bone appears red, cells are blue, and residual CM particles appear black. BG particles do not stain and appear white or gray. No residual polymer was observed in any of the sections, suggesting that it had completely degraded by 16 weeks. Similar to the μCT images (Fig. 3), the histological sections showed more new bone formation in the high-dose groups (Fig. 5A). Few BG particles were observed, suggesting that the BG had been substantially resorbed by 16 months. In contrast, residual CM particles were observed within the defect site for the LV/CM groups. Appositional new bone growth was observed near the surface of the CM particles, suggesting that the matrix functioned as a scaffold for bone formation. Residual ceramic particles were embedded in new bone. Osteoid was also observed near the ceramic–bone interface, providing evidence of active remodeling.

Ridge height in the defect area was measured from histological sections and compared to the same data obtained from μCT (Fig. 5B). The high-dose treatment groups exhibited significantly higher ridge heights compared to the low-dose groups for both μCT and histological methods. The Bland–Altman plot, which tests for differences between the μCT and histomorphometric measurements as a function of sample mean, showed no global differences between approaches within a 95% confidence interval (Fig. 5C).

Discussion

Ridge augmentation is a significant clinical challenge. Regeneration of alveolar bone is often required before implant placement in patients facing bone atrophy, tooth loss, or trauma, but there is no clinical standard of care for vertical ridge augmentation in patients. Previous studies have investigated GBR as a strategy for maintaining the volume of the bone defect and promoting new bone formation in vertical ridge augmentation models, but results from these studies have proven to be inconsistent, and complications have been reported, including wound failure, seroma, and graft exposure leading to infection.[16,22,23,33] In the present study, we hypothesized that injectable and settable bone

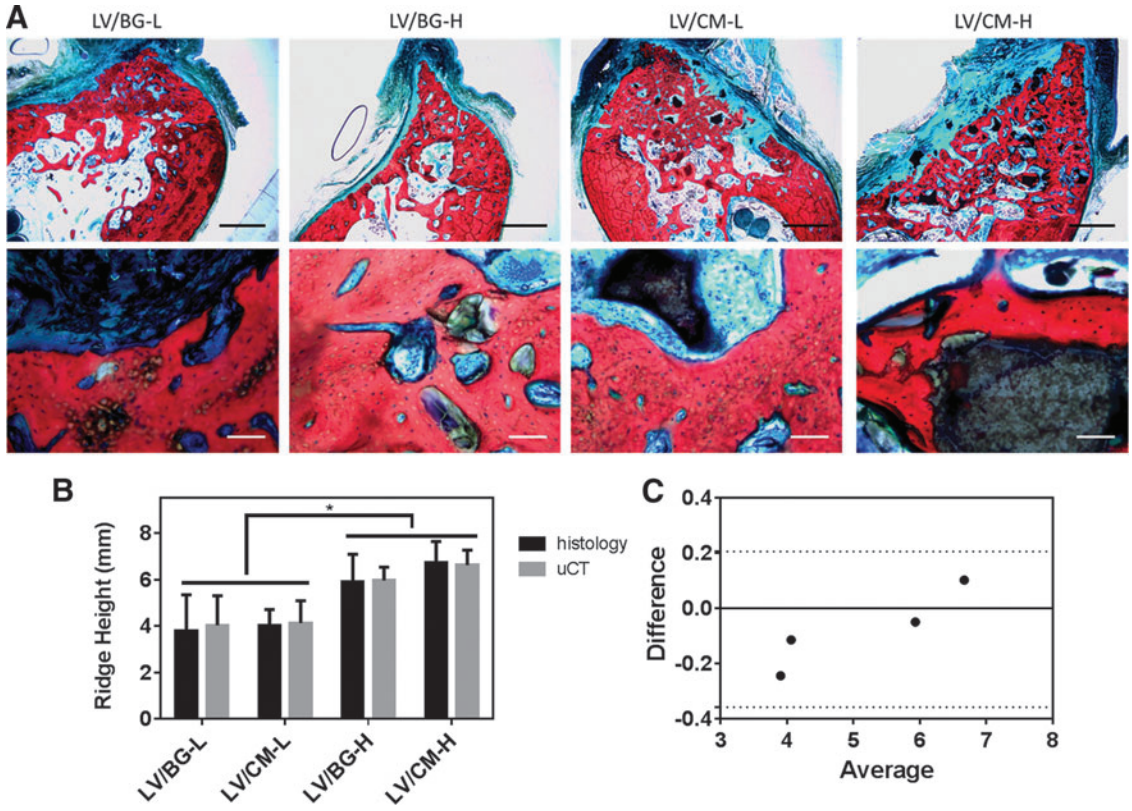

FIG. 5. Histological analysis of new bone formation and space maintenance. **(A)** Low-magnification (1.25×, scale bar = 2 mm, *top row*) and high-magnification (10×, scale bar = 0.1 mm, *bottom row*) images of histological sections show new bone formation (NB, *red*), infiltrating cells (*blue*), and osteoid (O) with residual CM (*black*) or BG (*clear*) particles. No residual polymer was observed. **(B)** Comparison of ridge height measured at the mesiodistal center of the defect from histological sections (*black bars*) and 2D μCT images (*gray bars*). Significant differences between low- and high-dose groups are denoted by $*p < 0.05$. **(C)** Bland–Altman plot shows no significant differences between the histological and μCT measurements of ridge height for each group with a 95% confidence interval (*dotted lines*). Color images available online at www.liebertpub.com/tea

grafts with bulk moduli exceeding that of the soft tissue would maintain space and support bone healing without the use of protective membranes. We found that LV grafts augmented with 400 μg/mL rhBMP-2 and initial bulk modulus exceeding 1.2 MPa maintained the initial width and height of the alveolar ridge, while the anatomic contour was not preserved at the low (100 μg/mL) dose.

To design compression-resistant grafts for ridge augmentation, it is important to know the critical bulk modulus of the graft required to maintain the anatomic contour of the ridge.[34,35] A recent study reported that an ACS carrier coated with poly(D,L-lactic-*co*-glycolic acid) maintained the contour ridge of the ridge and promoted new bone formation at an rhBMP-2 dose of 400 μg/mL dose.[36] However, the mechanical properties for this scaffold have not been reported. In the present study, both LV/BG (1.2 MPa) and LV/CM (3.1 MPa) composites maintained both the height and width of the mandibular ridge at the 400 μg/mL dose. The tensile and stress relaxation properties of porcine oral soft tissue have been recently characterized.[35,37] The Young's modulus of lingual and buccal attached gingiva ranges from 18.8 to 19.8 MPa, and the tensile strength ranges from 2.8 to 3.9 MPa.[35] These values are approximately one order of magnitude greater than those measured for LV grafts. GBR membranes, including chitosan (13–55 MPa),[38] poly(trimethylene carbonate) (5–7 MPa),[39] calcium sulfate/poly(β-amino ester) gels (100–400 MPa),[40] and starch/PCL scaffolds (34–45 MPa),[41] generally have moduli comparable to or exceeding that of human gingiva. The membranes protect the ACS, which has a Young's modulus of <0.1 MPa,[34,42] against compression by the adjacent tissue.[43]

Addition of ceramic particles to the ACS carrier maintained space and promoted new bone formation in porcine full-thickness mandibular defects without the protective titanium crib.[43] While the mechanical properties of the ceramic/collagen composite were not reported, a recent study has shown that addition of up to 80% HA to collagen scaffolds increases the bulk modulus to ~1 MPa.[42] These observations point to an initial bulk modulus of ~1 MPa as the lower limit for compression-resistant grafts in the mandibular ridge.

The effects of the composition of the ceramic particles on space maintenance and new bone formation in the mandibular ridge saddle defect model were also investigated. Two FDA-cleared synthetic ceramic bone graft substitutes were tested in this study: MASTERGRAFT Mini Granules (CM) and 45S5 Bioglass (BG) particles. CM particles were evaluated due to their compression-resistant and osteoconductive qualities when combined with the ACS carrier and rhBMP-2 in porcine mandibular continuity defects[43] and in posterolateral fusion both in nonhuman primates[44] and

humans.[45] Residual CM particles were present in the defect at 16 weeks, some of which were in the process of active remodeling with new bone growth appositional to the surface. These observations are consistent with a previous study evaluating CM/collagen composites augmented with rhBMP-2 in mandibular continuity defects in nonhuman primates.[43] In this study, a significant amount of residual CM was present at 6 months, most of which was in the process of active remodeling.[43] In contrast, minimal residual BG particles were present in the defect at 16 weeks (Fig. 5A) due to both the rapid resorption of BG particles by osteoclasts[46] and the dissolution products that stimulate osteoprogenitor cells.[4] Defects treated with LV/CM-H composites showed a modest increase in ridge width at 4 and 6 mm above the defect compared to LV/BG-H (Fig. 4A). However, no significant differences in ridge height measured in the middle of the defect were observed between the two groups (Fig. 5B, C). The modest differences in ridge width could result from differences in the initial bulk modulus of the composites and/or the degradation rate of the ceramic components.

While the ceramic composition exhibited a modest effect on new bone formation and space maintenance, the concentration of rhBMP-2 affected new bone formation in a dose-responsive manner. The high dose of rhBMP-2 was selected on the basis that it is at the high end of the recommended dose range for dogs (200–400 μg/mL).[47] The ridge height at the center of the defect was ≥6 mm for the high-dose groups compared to ≤4 mm for the low-dose groups (Fig. 5B). The Bland–Altman plot shows that the μCT and histological methods for measuring ridge height yield results that are statistically the same, which suggests that the new μCT method reported in this study is an appropriate method for measuring ridge height compared to the more conventional but time-consuming histological approach. Furthermore, the ridge width was maintained near the upper surface of the defect for the high-dose groups, while the low-dose groups revealed a trend of narrowing ridge width (Fig. 4A).

LV composites exhibit diffusion- and degradation-mediated rhBMP-2 for up to 4 weeks *in vivo*.[8] Considering previous studies reporting that a sustained release of rhBMP-2 can promote new bone formation at a suboptimal dose of rhBMP-2 in femoral segmental defects,[48,49] the low dose was anticipated to more effectively heal the ridge defects. Inadequate healing of the low-dose treatment groups in the present study could be attributed to the challenges of the mandibular ridge defect model, in which the graft is subject to compressive forces that are greater than the forces on the graft in the femoral segmental defect model. While the low-dose treatment did not maintain the host ridge height, the quality of the new bone that formed was similar to that observed for the high-dose treatment, as evidenced by the fact that no significant differences were observed between any of the morphometric parameters (BV/TV, Tb.N., Tb.Sp., or Tb.Th.) calculated from the μCT data for the low- and high-dose groups.

In previous studies, compression-resistant CM/collagen grafts maintained space and supported new bone formation in nonhuman primate posterolateral fusion[50] and mandibular continuity defect[43] models without protective membranes. However, the optimal dose for bone healing was 2.0 mg/mL, which was 33% higher than the recommended dose for the ACS carrier (1.5 mg/mL). In contrast, the LV/CM and LV/BG carriers supported new bone formation at a dose within the recommended range for dogs. Additional testing in a nonhuman primate model of lateral ridge augmentation is required to determine whether adequate space maintenance and bone healing can be achieved at a dose lower than that of the compression-resistant CM/collagen carrier.

This study was designed to answer the question whether injectable LV PUR/ceramic composites augmented with rhBMP-2 could maintain the contour of the ridge and promote bone healing in a large animal model of ridge augmentation at a clinically relevant time point. Both LV/BG and LV/CM grafts promoted new bone formation and maintained ridge height and width at the high dose of rhBMP-2 at 16 weeks. No residual polymer was observed in any of the four treatment groups, which is consistent with previous studies reporting that lysine-derived PURs undergo cell-mediated degradation[51] and almost completely degrade at 12 weeks in rabbit models of bone regeneration.[7,31] Images of histological sections (Fig. 5B) show appositional new bone growth on the surface of the CM particles. Thus, increasing the volume fraction of CM particles is anticipated to increase new bone formation, although the resulting composite would have limited injectability.[31,52]

Assessing outcomes at an intermediate (e.g., 8 weeks) time point could provide additional insight into the spatiotemporal dynamics of bone healing, specifically the relative contributions of the polymer and ceramic degradation rates to new bone formation.[53] Another limitation of this study is that the LV grafts were not compared to a clinical control, such as autograft or ACS. However, to our knowledge, this is the first study to report an injectable, settable, and compression-resistant bone graft that maintains the height and width of the mandibular ridge in a model in which conventional grafts, such as the ACS carrier[54–56] and autograft,[57] resorb without GBR membranes. In ongoing studies, the injectable LV/CM graft without a GBR membrane will be compared to the ACS carrier with the membrane in a preclinical model of lateral ridge augmentation to assess its potential as a compression-resistant carrier for rhBMP-2.

Conclusions

Injectable, settable, and compression-resistant LV bone grafts augmented with rhBMP-2 were evaluated in a canine mandibular ridge saddle defect model. Composite bone grafts synthesized from a lysine-derived PUR and ceramic particles exhibited bulk moduli exceeding 1 MPa. At the rhBMP-2 dose recommended for the ACS carrier in dogs (400 μg/mL), LV grafts maintained the width and height of the host mandibular ridge and supported new bone formation, while at suboptimal (100 μg/mL) doses, the anatomic contour of the ridge was not maintained. These findings suggest that both the initial bulk modulus and the rhBMP-2 dose regulate healing of compression-resistant bone grafts for healing mandibular ridge defects.

Acknowledgments

This material is based in part on work supported by the National Science Foundation under grant number 0847711

(CAREER award to S.A.G.). Any opinions, findings, and conclusions or recommendations expressed in this material are those of the author(s) and do not necessarily reflect the views of the National Science Foundation. This work was supported by the Army, Navy, NIH, Air Force, VA, and Health Affairs to support the AFIRM II effort under award no. W81XWH-14-2-0004. The U.S. Army Medical Research Acquisition Activity, 820 Chandler Street, Fort Detrick, MD 21702-5014 is the awarding and administering acquisition office. Opinions, interpretations, conclusions, and recommendations are those of the author and are not necessarily endorsed by the Department of Defense. A.D.T. acknowledges support from the Department of Education for a Graduate Assistance in Areas of National Need Fellowship under grant number P200A090323. Instrumentation for μCT analysis was purchased with funds from the NIH grant S10RR027631.

Disclosure Statement

S.A.G. is a consultant for Medtronic Spinal (Memphis, TN). All other authors have no competing financial interest to disclose.

References

1. Esposito, M., Grusovin, M.G., Felice, P., Karatzopoulos, G., Worthington, H.V., and Coulthard, P. Interventions for replacing missing teeth: horizontal and vertical bone augmentation techniques for dental implant treatment. Cochrane Database Syst Rev CD003607, 2009; DOI: 10.1002/14651858.CD003607.pub4.
2. Demarosi, F., Leghissa, G.C., Sardella, A., Lodi, G., and Carrassi, A. Localised maxillary ridge expansion with simultaneous implant placement: a case series. Br J Oral Maxillofac Surg **47,** 535, 2009.
3. Bohner, M., Galea, L., and Doebelin, N. Calcium phosphate bone graft substitutes: failures and hopes. J Eur Ceram Soc **32,** 2663, 2012.
4. Jones, J.R. Review of bioactive glass: from Hench to hybrids. Acta Biomater **9,** 4457, 2013.
5. Rezwan, K., Chen, Q.Z., Blaker, J.J., and Boccaccini, A.R. Biodegradable and bioactive porous polymer/inorganic composite scaffolds for bone tissue engineering. Biomaterials **27,** 3413, 2006.
6. Bonzani, I.C., Adhikari, R., Houshyar, S., Mayadunne, R., Gunatillake, P., and Stevens, M.M. Synthesis of two-component injectable polyurethanes for bone tissue engineering. Biomaterials **28,** 423, 2007.
7. Dumas, J.E., BrownBaer, P.B., Prieto, E.M., Guda, T., Hale, R.G., Wenke, J.C., and Guelcher, S.A. Injectable reactive biocomposites for bone healing in critical-size rabbit calvarial defects. Biomed Mater **7,** 024112, 2012.
8. Talley, A.D., Funk, S.S., Zienkiewicz, K.J., Dasgupta, J., Wenke, J.C., Davidson, J.M., Holt, G.E., and Guelcher, S.A. *In vivo* rhBMP-2 Release from Degradable Polyurethane Composites. Eur Cells Mater **28 (Suppl. 1),** 52, 2014.
9. Dumas, J.E., Davis, T., Holt, G.E., Yoshii, T., Perrien, D.S., Nyman, J.S., Boyce, T., and Guelcher, S.A. Synthesis, characterization, and remodeling of weight-bearing allograft bone/polyurethane composites in the rabbit. Acta Biomater **6,** 2394, 2010.
10. Harmata, A.J., Ward, C.L., Zienkiewicz, K.J., Wenke, J.C., and Guelcher, S.A. Investigating the effects of surface-initiated polymerization of ε-caprolactone to bioactive glass particles on the mechanical properties of settable polymer/ceramic composites. J Mater Res **29,** 2398, 2014.
11. Ji, W., Wang, H., van den Beucken, J.J.J.P., Yang, F., Walboomers, X.F., Leeuwenburgh, S., and Jansen, J.A. Local delivery of small and large biomolecules in craniomaxillofacial bone. Adv Drug Deliv Rev **64,** 1152, 2012.
12. Luvizuto, E.R., Tangl, S., Zanoni, G., Okamoto, T., Sonoda, C.K., Gruber, R., and Okamoto, R. The effect of BMP-2 on the osteoconductive properties of β-tricalcium phosphate in rat calvaria defects. Biomaterials **32,** 3855, 2011.
13. Notodihardjo, F.Z., Kakudo, N., Kushida, S., Suzuki, K., and Kusumoto, K. Bone regeneration with BMP-2 and hydroxyapatite in critical-size calvarial defects in rats. J Craniomaxillofac Surg **40,** 287, 2012.
14. Mariner, P.D., Wudel, J.M., Miller, D.E., Genova, E.E., Streubel, S.O., and Anseth, K.S. Synthetic hydrogel scaffold is an effective vehicle for delivery of INFUSE (rhBMP2) to critical-sized calvaria bone defects in rats. J Orthop Res **31,** 401, 2013.
15. Jung, R.E., Weber, F.E., Thoma, D.S., Ehrbar, M., Cochran, D.L., and Hämmerle, C.H.F. Bone morphogenetic protein-2 enhances bone formation when delivered by a synthetic matrix containing hydroxyapatite/tricalciumphosphate. Clin Oral Implants Res **19,** 188, 2008.
16. Jovanovic, S.A., Hunt, D.R., Bernard, G.W., Spiekermann, H., Wozney, J.M., and Wikesjo, U.M. Bone reconstruction following implantation of rhBMP-2 and guided bone regeneration in canine alveolar ridge defects. Clin Oral Implants Res **18,** 224, 2007.
17. Huh, J.-B., Kim, S.-E., Kim, H.-E., Kang, S.-S., Choi, K.-H., Jeong, C.-M., Lee, J.-Y., and Shin, S.-W. Effects of anodized implants coated with *Escherichia coli*-derived rhBMP-2 in beagle dogs. Int J Oral Maxillofac Surg **41,** 1577, 2012.
18. de Freitas, R.M., Spin-Neto, R., Junior, E.M., Pereira, L.A.V.D., Wikesjö, U.M.E., and Susin, C. Alveolar ridge and maxillary sinus augmentation using rhBMP-2: a systematic review. Clin Implant Dent Relat Res **17,** e192, 2015.
19. Schwarz, F., Mihatovic, I., Golubovic, V., Hegewald, A., and Becker, J. Influence of two barrier membranes on staged guided bone regeneration and osseointegration of titanium implants in dogs: part 1. Augmentation using bone graft substitutes and autogenous bone. Clin Oral Implants Res **23,** 83, 2012.
20. Iglhaut, G., Schwarz, F., Grundel, M., Mihatovic, I., Becker, J., and Schliephake, H. Shell technique using a rigid resorbable barrier system for localized alveolar ridge augmentation. Clin Oral Implants Res **25,** e149, 2014.
21. Ruskin, J.D., Hardwick, R., Buser, D., Dahlin, C., and Schenk, R.K. Alveolar ridge repair in a canine model using rhTGF-β1 with barrier membranes. Clin Oral Implants Res **11,** 107, 2000.
22. Schliephake, H., Drewes, M., Mihatovic, I., Schwarz, F., Becker, J., and Iglhaut, G. Use of a self-curing resorbable polymer in vertical ridge augmentations—a pilot study in dogs. Clin Oral Implants Res **25,** 435, 2014.
23. dal Polo, M.R., Poli, P.P., Rancitelli, D., Beretta, M., and Maiorana, C. Alveolar ridge reconstruction with titanium meshes: a systematic review of the literature. Med Oral Patol Oral Cir Bucal **19,** e639, 2014.
24. Guelcher, S., Srinivasan, A., Hafeman, A., Gallagher, K., Doctor, J., Khetan, S., McBride, S., and Hollinger, J.

Synthesis, in vitro degradation, and mechanical properties of two-component poly(ester urethane)urea scaffolds: effects of water and polyol composition. Tissue Eng **13,** 2321, 2007.
25. Guelcher, S.A., Patel, V., Gallagher, K.M., Connolly, S., Didier, J.E., Doctor, J.S., and Hollinger, J.O. Synthesis and in vitro biocompatibility of injectable polyurethane foam scaffolds. Tissue Eng **12,** 1247, 2006.
26. Jiang, G., Evans, M., Jones, I., Rudd, C., Scotchford, C., and Walker, G. Preparation of poly (ε-caprolactone)/continuous bioglass fibre composite using monomer transfer moulding for bone implant. Biomaterials **26,** 2281, 2005.
27. Jiang, G., Walker, G., Jones, I., and Rudd, C. XPS identification of surface-initiated polymerisation during monomer transfer moulding of poly (ε-caprolactone)/Bioglass® fibre composite. Appl Surf Sci **252,** 1854, 2005.
28. Verné, E., Vitale-Brovarone, C., Bui, E., Bianchi, C., and Boccaccini, A. Surface functionalization of bioactive glasses. J Biomed Mater Res A **90,** 981, 2009.
29. Bouxsein, M.L., Boyd, S.K., Christiansen, B.A., Guldberg, R.E., Jepsen, K.J., and Muller, R. Guidelines for assessment of bone microstructure in rodents using micro-computed tomography. J Bone Miner Res **25,** 1468, 2010.
30. Hoshi, S., Akizuki, T., Matsuura, T., Ikawa, T., Kinoshita, A., Oda, S., Tabata, Y., Matsui, M., and Izumi, Y. Ridge augmentation using recombinant human fibroblast growth factor-2 with biodegradable gelatin sponges incorporating β-tricalcium phosphate: a preclinical study in dogs. J Periodontal Res **51,** 77, 2016.
31. Prieto, E.M., Talley, A.D., Gould, N.R., Zienkiewicz, K.J., Drapeau, S.J., Kalpakci, K.N., and Guelcher, S.A. Effects of particle size and porosity on *in vivo* remodeling of settable allograft bone/polymer composites. J Biomed Mater Res B Appl Biomater **103,** 1641, 2015.
32. Dumas, J.E., Zienkiewicz, K., Tanner, S.A., Prieto, E.M., Bhattacharyya, S., and Guelcher, S.A. Synthesis and characterization of an injectable allograft bone/polymer composite bone void filler with tunable mechanical properties. Tissue Eng Part A **16,** 2505, 2010.
33. Verardi, S., and Simion, M. Management of the exposure of e-PTFE membranes in guided bone regeneration. Pract Proced Aesthet Dent **19,** 111, 2007.
34. Hyder, P., Dowell, P., Singh, G., and Dolby, A. Freeze-dried, cross-linked bovine type I collagen: analysis of properties. J Periodontol **63,** 182, 1992.
35. Goktas, S., Dmytryk, J.J., and McFetridge, P.S. Biomechanical behavior of oral soft tissues. J Periodontol **82,** 1178, 2011.
36. Kawakatsu, N., Oda, S., Kinoshita, A., Kikuchi, S., Tsuchioka, H., Akizuki, T., Hayashi, C., Kokubo, S., Ishikawa, I., and Izumi, Y. Effect of rhBMP-2 with PLGA/gelatin sponge type (PGS) carrier on alveolar ridge augmentation in dogs. J Oral Rehabil **35,** 647, 2008.
37. Lacoste-Ferré, M.-H., Demont, P., Dandurand, J., Dantras, E., Duran, D., and Lacabanne, C. Dynamic mechanical properties of oral mucosa: comparison with polymeric soft denture liners. J Mech Behav Biomed Mater **4,** 269, 2011.
38. Xu, C., Lei, C., Meng, L., Wang, C., and Song, Y. Chitosan as a barrier membrane material in periodontal tissue regeneration. J Biomed Mater Res B Appl Biomater **100B,** 1435, 2012.
39. van Leeuwen, A.C., Huddleston Slater, J.J.R., Gielkens, P.F.M., de Jong, J.R., Grijpma, D.W., and Bos, R.R.M. Guided bone regeneration in rat mandibular defects using resorbable poly(trimethylene carbonate) barrier membranes. Acta Biomater **8,** 1422, 2012.
40. Orellana, B.R., Thomas, M.V., Dziubla, T.D., Shah, N.M., Hilt, J.Z., and Puleo, D.A. Bioerodible calcium sulfate/poly(β-amino ester) hydrogel composites. J Mech Behav Biomed Mater **26,** 43, 2013.
41. Requicha, J.F., Viegas, C.A., Hede, S., Leonor, I.B., Reis, R.L., and Gomes, M.E. Design and characterization of a biodegradable double-layer scaffold aimed at periodontal tissue-engineering applications. J Tissue Eng Regen Med 2013 [Epub ahead of print]; DOI: 10.1002/term .1816.
42. Kane, R.J., Weiss-Bilka, H.E., Meagher, M.J., Liu, Y., Gargac, J.A., Niebur, G.L., Wagner, D.R., and Roeder, R.K. Hydroxyapatite reinforced collagen scaffolds with improved architecture and mechanical properties. Acta Biomater **17,** 16, 2015.
43. Herford, A.S., Lu, M., Buxton, A.N., Kim, J., Henkin, J., Boyne, P.J., Caruso, J.M., Rungcharassaeng, K., and Hong, J. Recombinant human bone morphogenetic protein 2 combined with an osteoconductive bulking agent for mandibular continuity defects in nonhuman primates. J Oral Maxillofac Surg **70,** 703, 2012.
44. Akamaru, T., Suh, D., Boden, S.D., Kim, H.S., Minamide, A., and Louis-Ugbo, J. Simple carrier matrix modifications can enhance delivery of recombinant human bone morphogenetic protein-2 for posterolateral spine fusion. Spine (Phila Pa 1976) **28,** 429, 2003.
45. Dawson, E., Bae, H.W., Burkus, J.K., Stambough, J.L., and Glassman, S.D. Recombinant human bone morphogenetic protein-2 on an absorbable collagen sponge with an osteoconductive bulking agent in posterolateral arthrodesis with instrumentation. J Bone Joint Surg Am **91,** 1604, 2009.
46. Midha, S., van den Bergh, W., Kim, T.B., Lee, P.D., Jones, J.R., and Mitchell, C.A. Bioactive glass foam scaffolds are remodelled by osteoclasts and support the formation of mineralized matrix and vascular networks in vitro. Adv Healthc Mater **2,** 490, 2013.
47. McKay, W.F., Peckham, S.M., and Marotta, J.S. The Science of rhBMP-2. St. Louis, MO: Quality Medical Publishing, 2006.
48. Brown, K.V., Li, B., Guda, T., Perrien, D.S., Guelcher, S.A., and Wenke, J.C. Improving bone formation in a rat femur segmental defect by controlling bone morphogenetic protein-2 release. Tissue Eng Part A **17,** 1735, 2011.
49. Boerckel, J.D., Kolambkar, Y.M., Dupont, K.M., Uhrig, B.A., Phelps, E.A., Stevens, H.Y., Garcia, A.J., and Guldberg, R.E. Effects of protein dose and delivery system on BMP-mediated bone regeneration. Biomaterials **32,** 5241, 2011.
50. Barnes, B., Boden, S.D., Louis-Ugbo, J., Tomak, P.R., Park, J.S., Park, M.S., and Minamide, A. Lower dose of rhBMP-2 achieves spine fusion when combined with an osteoconductive bulking agent in non-human primates. Spine (Phila Pa 1976) **30,** 1127, 2005.
51. Hafeman, A.E., Zienkiewicz, K.J., Zachman, A.L., Sung, H.J., Nanney, L.B., Davidson, J.M., and Guelcher, S.A. Characterization of the degradation mechanisms of lysine-derived aliphatic poly(ester urethane) scaffolds. Biomaterials **32,** 419, 2011.
52. Bennett, S., Connolly, K., Lee, D.R., Jiang, Y., Buck, D., Hollinger, J.O., and Gruskin, E.A. Initial biocompatibility

studies of a novel degradable polymeric bone substitute that hardens in situ. Bone **19,** S101, 1996.
53. Dumas, J.E., Prieto, E.M., Zienkiewicz, K.J., Guda, T., Wenke, J.C., Bible, J., Holt, G.E., and Guelcher, S.A. Balancing the rates of new bone formation and polymer degradation enhances healing of weight-bearing allograft/polyurethane composites in rabbit femoral defects. Tissue Eng Part A **20,** 115, 2014.
54. Sigurdsson, T.J., Nygaard, L., Tatakis, D.N., Fu, E., Turek, T.J., Jin, L., Wozney, J.M., and Wikesjö, U. Periodontal repair in dogs: evaluation of rhBMP-2 carriers. Int J Periodontics Restorative Dent **16,** 524, 1996.
55. Barboza, E.P., Caúla, A.L., Caúla Fde, O., de Souza, R.O., Neto, L.G., Sorensen, R.G., Li, X.J., and Wikesjö, U.M. Effect of recombinant human bone morphogenetic protein-2 in an absorbable collagen sponge with space-providing biomaterials on the augmentation of chronic alveolar ridge defects. J Periodontol **75,** 702, 2004.
56. Barboza, E.P., Duarte, M.E.L., Geolás, L., Sorensen, R.G., Riedel, G.E., and Wikesjö, U.M. Ridge augmentation following implantation of recombinant human bone morphogenetic protein-2 in the dog. J Periodontol **71,** 488, 2000.
57. Von Arx, T., Schenk, R.K., Buser, D., Cochran, D.L., and Hermann, J.S. Lateral ridge augmentation using different bone fillers and barrier membrane application. Clin Oral Implants Res **12,** 260, 2001.

Address correspondence to:
Scott A. Guelcher, PhD
Department of Chemical and Biomolecular Engineering
Vanderbilt University
PMB #351604
2301 Vanderbilt Place
Nashville, TN 37235

E-mail: scott.guelcher@vanderbilt.edu

Received: July 31, 2015
Accepted: January 19, 2016
Online Publication Date: February 29, 2016